



HAL
open science

A fast and low-cost dynamic calorimetric method for phase diagram estimation of binary systems

Clément Mailhe, Marie Duquesne

► **To cite this version:**

Clément Mailhe, Marie Duquesne. A fast and low-cost dynamic calorimetric method for phase diagram estimation of binary systems. *Journal of Thermal Analysis and Calorimetry*, 2020, 143, pp.587-598. 10.1007/s10973-020-09287-6 . hal-03377523

HAL Id: hal-03377523

<https://hal.science/hal-03377523>

Submitted on 14 Oct 2021

HAL is a multi-disciplinary open access archive for the deposit and dissemination of scientific research documents, whether they are published or not. The documents may come from teaching and research institutions in France or abroad, or from public or private research centers.

L'archive ouverte pluridisciplinaire **HAL**, est destinée au dépôt et à la diffusion de documents scientifiques de niveau recherche, publiés ou non, émanant des établissements d'enseignement et de recherche français ou étrangers, des laboratoires publics ou privés.

A fast and low-cost dynamic calorimetric method for phase diagram estimation of binary systems

Clément Mailhé¹  · Marie Duquesne² 

Abstract

A dynamic calorimetric method based on infrared thermography has been used for the phase diagram estimation of binary systems of fatty organic materials. Its promising results make of this innovative method an interesting asset in applications with time constraints. In order to provide a calorimetry method with satisfactory performance and the lowest time consumption and cost, a test campaign is undergoing. This campaign aims at evaluating the influence of operating conditions on the performances of the method. In that frame, the phase diagrams estimated using a high-end photon detector and a low-cost microbolometer are compared. The assessment of the accuracy and reliability of phase transitions detection is made based on the study of 4 binary systems of fatty acids and fatty alcohols. Differential scanning calorimetry is used for the validation of the experimental phase diagram, and further works are identified in the light of innovative data obtained using the infrared thermography method.

Keywords Screening · Infrared thermography · Phase diagram · Phase transitions · Fatty organic materials

Introduction

Phase diagrams are compulsory tools and essential assets in material synthesis, thermodynamic modeling as well as for the study of materials behavior and properties [1–4]. Standard calorimetric methods for phase diagram establishment either involve following a material property while submitted to a heating ramp (differential thermal analysis, differential scanning calorimetry, etc.) or observing a sample under thermodynamic equilibrium (X-ray powder diffraction, scanning electron microscopy, etc.). The mentioned methods are complementary, and allow through their combined use, the establishment of accurate and reliable phase diagrams. However, the cost of these methods is high and

their ability to only test one sample at a time makes the phase diagram establishment process a very time-consuming task. In some applications, such as material synthesis or material screening, this time constraint is a drag. The screening procedures imply sampling numerous compositions of multi-component systems, until the identification of a candidate matching the required specifications. In order to accelerate this process and consequently facilitate the development of new materials, a new method based on infrared thermography was developed. This innovative experimental method allows the estimation in a few hours only of a complete phase diagram when standard methods require days to weeks. The approached phase diagram provided by this method allows rapidly identifying compositions or areas of interest to be precisely investigated with the use of the aforementioned standard methods. The concept and applicability of this method has already been successfully demonstrated for the phase diagram estimation of binary systems of sugar alcohols [5] and fatty acids [6]. Given the promising results provided by the infrared thermography (IRT) method, an extensive assessment of the influence of experimental parameters is performed in order to identify the configuration as cheap, accurate and fast as possible. A step toward the optimization of this method was already performed in [7] where improvements to the method are proposed through a

Electronic supplementary material The online version of this article (<https://doi.org/10.1007/s10973-020-09287-6>) contains supplementary material, which is available to authorized users.

✉ Clément Mailhé
clement.mailhe@u-bordeaux.fr

¹ CNRS, I2M Bordeaux, Université de Bordeaux, Esplanade des Arts et Métiers, 33405 Talence Cedex, France

² CNRS, I2M Bordeaux, Bordeaux INP, Esplanade des Arts et Métiers, 33405 Talence Cedex, France

parametric study and the automation of the data treatment process. An essential equipment in the use of this method is the infrared imaging device. Numerous infrared detectors with different types, characteristics and prices range exist. For an optimal selection of the device, an evaluation of the cameras performances based on the provided results must be made in order to obtain a method providing satisfactory results for the lowest cost and time consumption. In this work, two infrared cameras are compared with significantly different specifications. The performances and the influence of cameras parameters are evaluated upon comparison of the phase diagrams obtained using the IRT method for both cameras and for 4 binary systems of fatty acids and fatty alcohols with a growing complexity. In addition, the accuracy of the results is also assessed in comparison with standard methods data provided by DSC measurements and extracted from literature.

Materials and methods

IRT method

The IRT method is classified as a dynamic calorimetric method such as differential scanning calorimetry (DSC) and differential thermal analysis (DTA). Its principle has already been discussed in [5–7]. It relies on the monitoring of the photonic flux emitted by droplets, each of them having a given molar composition. These droplets are deposited on

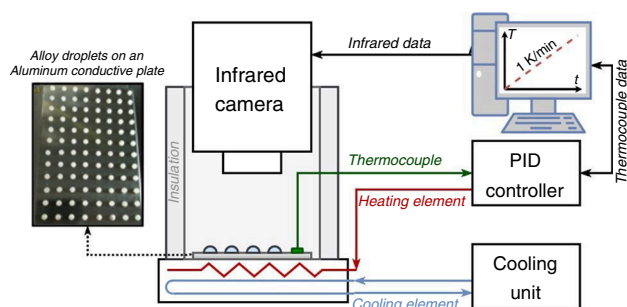


Fig. 1 Scheme of the IRT method experimental setup

a conductive aluminum plate and are submitted to a heating ramp at a controlled rate of $1\text{ }^{\circ}\text{C min}^{-1}$. Figure 1 illustrates the experimental setup developed for this method. As a phase transition is accompanied by a modification of the structure of the material, the droplet emissivity is modified during its phase change. This phenomenon is associated with an abrupt variation of the monitored photonic flux. It is therefore possible to simultaneously keep track of phase transitions for as many samples as there are droplets on the conductive plate. The phase diagram estimation process duration is consequently reduced by at least a factor corresponding to the number of droplets.

Samples

The 4 binary systems studied in this work are: palmitic acid + stearic acid, 1-hexadecanol + myristic acid, 1-hexadecanol + 1-octadecanol and myristic acid + stearic acid. All studied compounds are fatty acids and fatty alcohols. Either biosourced or by-products of biosourced materials, their large bioavailability [8, 9] and their range of applications such as in the food, pharmaceutical or energy (biofuel, thermal energy storage, etc.) industries make their study and the understanding of their properties an important topic [10]. This aspect is indeed highlighted by the many research works exploring the application of biosourced organic materials [11–14]. The key thermal properties and characteristics of the pure materials are listed in Table 1.

For the 4 considered systems, 3 sets of experiments are performed. For the first series of experiments, the phase diagrams of the 4 systems are plotted using a high-end camera, identical to the one used in [5–7]. The phase diagrams are obtained for the study of 101 droplets with molar compositions ranging from 0 to 100% by 1% increments. The second series of experiments aims at verifying the applicability of the IRT method for phase diagrams estimations using a low-cost camera. For the latter series, the phase diagrams of the HD + MA and PA + SA binary systems are estimated from the study of 21 droplets only with molar compositions ranging from 0 to 100% by 5% increments. This set is performed in order to check if phase diagrams could be estimated using this new camera. Once verified that the low-cost camera

Table 1 Characteristics and thermal properties of the pure studied materials

	Myristic acid	Palmitic acid	Stearic acid	1-Hexadecanol	1-Octadecanol
CAS number	544-63-8	57-10-3	57-11-4	36653-82-4	112-92-5
Acronym	MA	PA	SA	HD	OD
Formula	$\text{C}_{14}\text{H}_{28}\text{O}_2$	$\text{C}_{16}\text{H}_{32}\text{O}_2$	$\text{C}_{18}\text{H}_{36}\text{O}_2$	$\text{C}_{16}\text{H}_{34}\text{O}$	$\text{C}_{18}\text{H}_{38}\text{O}$
Molar mass/g mol ⁻¹	228.37	256.43	284.48	242.44	270.49
Melting temperature/ $^{\circ}\text{C}$	53.74–54.84	61.5	68.9–69.41	48.28	56.34
Supplier	Sigma-Aldrich	Sigma-Aldrich	Sigma-Aldrich	Sigma-Aldrich	Sigma-Aldrich
Purity	> 99%	> 99%	> 98.5%	99%	99%

provides good estimations, a third series is performed for the remaining 2 systems but once again for the study of 101 droplets.

Infrared cameras

The infrared cameras used in this study are the FLIR X6580 SC and the OPTRIS PI 450. Both present significant differences. The FLIR one being a high-end infrared imaging device for advanced R&D applications, while the OPTRIS camera is an entry-range, low-cost camera estimated to be approximately 15 times cheaper than the previous one (and 3–4 times cheaper than an entry-range DSC). The subsections hereafter present their essential characteristics and an evaluation of their supposed impact on the results provided by the IRT method. The specifications of both cameras are available in Table 2 and were provided by the manufacturer unless stated otherwise.

FLIR X6580 SC

The FLIR X6580 SC is a cooled photon detector with an indium antimonide (InSb) detector material. It allows acquisition rates up to 355 Hz at a nominal resolution of 640×512 pixels. Regarding its accuracy, it is expected to provide a high signal-to-noise ratio (SNR) with a typical noise equivalent temperature deviation (NETD) of only 18 mK and precise reading geometrically as well as value-wise with a small detector pitch of $15 \mu\text{m}$. It also has a nominal deviation evaluated at $\pm 1 \text{ }^\circ\text{C}$ or $\pm 1\%$. This camera includes a large integration time ranging from 0.5 up to 20,000 μs allowing for a high responsivity. Typical integration times for this particular application range from 600 to 1000 μs . The spectral

range of the detector is between 1.5 and $5.4 \mu\text{m}$, and it is calibrated in the $5\text{--}300 \text{ }^\circ\text{C}$ range.

OPTRIS PI 450

The OPTRIS PI 450 is an uncooled microbolometer. It allows for acquisition rates up to 80 Hz at a nominal resolution of 388×288 pixels. Regarding the accuracy and sensitivity of the low-cost camera, the NETD is about twice higher at 40 mK and the detector pitch is sensibly the same with only $17 \mu\text{m}$. The reading accuracy is also evaluated to be twice the one of the FLIR camera. The responsivity of the microbolometer is evaluated in terms of thermal time constants and corresponds to the time necessary for the infrared imaging device to notice a variation. This fixed parameter is not provided by the manufacturer, but typical values found in the literature are 8–10 ms [15, 16]. The spectral range of this camera is between 7.5 and $13 \mu\text{m}$, and it includes three temperature ranges: -20 to $100 \text{ }^\circ\text{C}$, $0\text{--}250 \text{ }^\circ\text{C}$ and $150\text{--}900 \text{ }^\circ\text{C}$.

Properties comparison and performances assessment

Cooled photon detectors are highly recommended for dynamic applications [15] where high sensitivities, frame rates and resolutions can be provided when uncooled thermal detector cannot. However, the principle of the IRT method implies a slow paced heating of non-moving samples whose observation is made at a macroscopic scale. In that frame, it is unsure whether the level of performance provided by the FLIR camera is needed or if an entry-range microbolometer can be competitive for phase diagrams estimations.

The FLIR detector is able to provide 3 times more pixels than the OPTRIS one. Although more data implies more data treatment, a more accurate reading of the photonic flux emitted by each droplet can be expected with the high-end camera. However, in a previous analysis [7], the influence of the droplet size on the results provided by the IRT method was assessed. The study showed that phase diagrams obtained for droplets with 3 mm and 7 mm diameters only presented small differences. The area occupied by a 7-mm-diameter droplet in the field of view is yet more than 5 times a 3-mm one. Therefore, it can be assumed that this difference in resolution will have a slight to no impact on the estimated phase diagrams. In that case, less data treatment for the same results favors the solution with the lowest resolution.

The FLIR camera is able to provide significantly higher frame rates at the nominal resolution than the OPTRIS microbolometer. However, the heating rate applied during the IRT experiment is of $1 \text{ }^\circ\text{C min}^{-1}$ (i.e., $0.017 \text{ }^\circ\text{C s}^{-1}$). Additionally, the PID temperature control is only able to provide a $0.1 \text{ }^\circ\text{C}$ reading accuracy. Consequently, given our temperature reading precision and our slow temperature ramp, it is unlikely that frame rates above 10 Hz bring

Table 2 Infrared cameras characteristics

Camera model	FLIR X6580 SC	OPTRIS PI 450
Resolution	640×512 pixels	382×288 pixels
Number of pixels	327 680	110 016
Detector type/material	InSb (middle wavelength photon detector)	Microbolometer (long wavelength detector)
Detector cooling	Yes ($-196 \text{ }^\circ\text{C}$)	No
Maximum frame rate/Hz	355	80
Spectral range/ μm	1.5–5.4	7.5–13
Integration time range/ μs —time constant/ μs	0.5–20,000	8000–10,000 ^a
Accuracy	$\pm 1 \text{ }^\circ\text{C}$ or $\pm 1\%$ of reading value	$\pm 2 \text{ }^\circ\text{C}$ or $\pm 2\%$ of reading value

^aData not provided. Indicated values are typical values for microbolometers [15, 16]

any additional relevant information. The acquisition rate is hence chosen so the amount of gathered data is limited to a required minimum.

Regarding the difference in spectral ranges in both cameras, according to Planck's law the spectral radiance is higher in the 7.5–13 μm spectral range than in the 1.5–5.4 μm at temperatures inferior to 150 $^{\circ}\text{C}$ [15, 17]. Although photon detectors are characterized by higher detectivities and hence better performances, the spectral range of the low cost camera may be an advantage whose importance will have to be assessed.

Lastly, as far as accuracy and reliability are concerned, we logically expect more noise with the results provided by the OPTRIS camera. However, it should be mentioned that the signal treatment and interpretation involved in the method and thoroughly detailed in [5] does not rely on reading a signal value itself but rather on a signal variation making the noise level and reading accuracy less impactful.

Differential scanning calorimetry

The results obtained using the IRT method are confronted to those of standard calorimetry methods either extracted from the literature or obtained from DSC analyses. The DSC analyses are performed at 2 different heating rates leading to 2 series of experiments. One with a 1 $^{\circ}\text{C min}^{-1}$ heating rate, matching the one used for the IRT method and one at a 0.3 $^{\circ}\text{C min}^{-1}$ heating rate in order to identify occurring transitions with close transition temperatures. In both series of experiments, samples ranging from 5 to 15 mg are weighed using a Mettler Toledo scale with a weighing accuracy of ± 0.03 mg. The exact mass of each sample is provided in the Supplementary material, together with the DSC transition data and examples of DSC curves highlighting presented results. The samples are placed in alumina crucibles for analysis. The determination of the transition temperature is performed following the guidelines stated in [18]. Hence, the considered transition temperature is either the calculated onset temperature if a flat baseline is clearly established or the peak temperature otherwise. The experiments are carried on with a DSC 131 provided by SETARAM, and the analysis software used is SETSOFT 2000. Its calibration is performed using gallium (purity: 99.9999%), indium (purity: 99.995%), tin (purity: 99.999%) and lead (purity: 99.999%) to validate the results precision in the 29.8–327.5 $^{\circ}\text{C}$ temperature range.

Results

The evaluation of the performances of both infrared cameras for phase diagram estimation using the IRT method is made upon comparison of phase diagrams obtained using

standard methods and the IRT method. Qualitatively, it is sought that the IRT method be able to detect most transitions found with standard methods, so a satisfactory depiction of the phase diagram of multi-component systems is rendered. Quantitatively, we identify phase transitions that were detected with both cameras and whose occurrence is confirmed at least twice by DSC measurements. To simplify the analysis, we make the distinction between 2 types of transitions: the liquidus line transition and the horizontal transitions (eutectic, peritectic, metatectic, etc.). For both, we assess the efficiency of the IRT method using both cameras for phase diagrams estimation at low to medium temperatures based on accuracy and reliability. For the accuracy, the transition temperature deviation between DSC measurements and IRT data is computed. For the reliability, we evaluate the standard deviation σ (calculated as stated in Eq. 1) over the n samples for which the transition is detected. The literature data are not considered for the quantitative comparison as differences in composition, purity of the compounds or even operating conditions may affect the results.

$$\sigma = \sqrt{\frac{\sum_{i=1}^n (T_i - \bar{T})^2}{n - 1}} \quad (1)$$

With \bar{T} the average transition temperature, T_i the transition temperature for the sample i , σ the standard deviation and n the number of samples for which the transition is detected.

Palmitic acid + stearic acid

The phase diagram obtained applying the IRT method using both cameras is plotted in Fig. 2 where it is compared to the phase diagram and the transitions detected with DSC measurements as well as in the literature [19]. The purity of the pure palmitic acid in the literature and in this work is comparable, but the stearic acid one is slightly better in the present study. As a result, DSC measurements and literature data may not fully coincide.

For the PA + SA binary system, the phase diagram depicted applying the IRT method, whether it is performed using the FLIR photon detector or the OPTRIS microbolometer is coherent with what standard methods can provide. All transitions detected by DSC were also consistently detected with the infrared cameras. In addition, we notice on both extremities of the IRT phase diagrams phases that resemble solid solubility domains whose presence is consistent with the phase diagram depicted by the authors in [19]. Their presence, however, needs to be nuanced as their occurrence still needs to be proven by the use of other complementary methods (X-ray diffraction for instance).

Fig. 2 Phase diagram of the PA+SA binary systems plotted using the IRT method and standard calorimetry methods

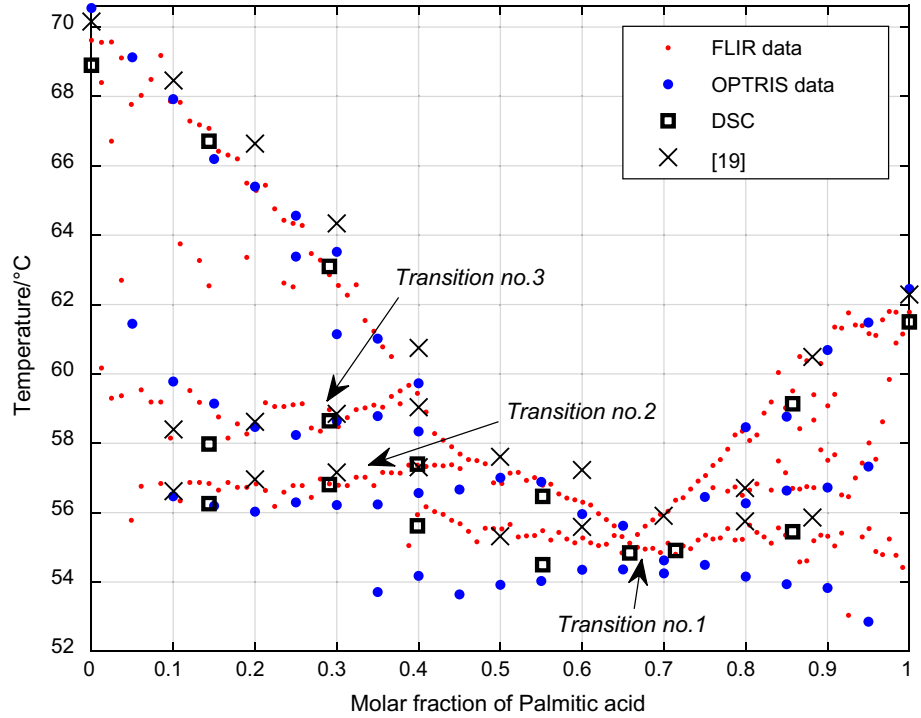


Table 3 Comparison of the horizontal transitions detection between the IRT method and DSC measurements for the PA+SA binary system

Transition no.	1	2	3
$\bar{T}_{DSC}/^{\circ}C$	55.064	56.823	58.315
$\sigma_{DSC}/^{\circ}C$	0.461	0.57	0.474
n	5	3	2
$\bar{T}_{OPTRIS}/^{\circ}C$	54.072	56.288	58.604
$\sigma_{OPTRIS}/^{\circ}C$	0.271	0.18	0.696
n	12	7	6
$\bar{T}_{FLIR}/^{\circ}C$	55.234	56.833	58.926
$\sigma_{FLIR}/^{\circ}C$	0.312	0.34	0.696
n	60	34	29

With \bar{T} the average transition temperature, σ the standard deviation and n the number of samples for which the transition is detected

The accuracy and reliability of the horizontal transitions and the liquidus line detection are, respectively, evaluated in Tables 3 and 4.

For the PA+SA binary system, the detection of 3 horizontal transitions is assessed. The absolute average temperature deviation between DSC measurements and the results provided by the IRT method using the OPTRIS microbolometer is 0.61 °C. On the other hand, the computed deviation for the FLIR results is estimated at 0.26 °C which shows here to be more precise although 0.61 °C temperature deviation is more than satisfactory for a first estimation. Regarding

Table 4 Comparison of the liquidus line detection between the IRT method and DSC measurements for the PA+SA binary system

Comparison	DSC/OPTRIS	DSC/FLIR	OPTRIS/FLIR
$\overline{\Delta T}/^{\circ}C$	0.858	0.674	0.53
$\sigma_{\overline{\Delta T}}/^{\circ}C$	0.696	0.64	0.41
$\Delta T_{max}/^{\circ}C$	2.33	2.04	1.605
$\Delta T_{min}/^{\circ}C$	0.286	0.24	0.043
n	9	9	21

With $\overline{\Delta T}$ the average liquidus temperature difference between methods, $\sigma_{\overline{\Delta T}}$ the standard deviation, ΔT_{max} and ΔT_{min} , respectively, the maximum and minimum liquidus temperature deviation between methods and n the number of samples for which data is available with both methods

the detection reliability, we notice that for both cameras, the standard deviation from the calculated mean transition temperature is good with values below or in the range of what the DSC provides. This reliability is especially satisfying considering that the detection is made for significantly more compositions than with the DSC.

The overall average temperature deviation for the liquidus line detection between DSC measurements and the IRT method using the OPTRIS camera and the FLIR camera is, respectively, 0.86 °C and 0.67 °C. Although the FLIR photon detector appears to be slightly more accurate, both provide very good approximations for the liquidus line depiction. As for the reliability of this detection, standard deviations show similar behaviors using both cameras and

remain relatively low. A comparative analysis between the results provided by the two cameras shows that the liquidus line for the OPTRIS camera is really close to the FLIR one with an average deviation of $0.53\text{ }^{\circ}\text{C}$ and that this deviation is relatively stable with a low measured standard deviation. It suggests that the liquidus lines depicted by both cameras are identical in shape and that a simple offset differentiate each other.

1-Hexadecanol + myristic acid

The phase diagram obtained applying the IRT method using both cameras is plotted in Fig. 3 where it is compared to the phase diagram and transitions detected with DSC measurements as well as in the literature [20]. The purity of both pure compounds in the literature and in this work is comparable.

As for the previous system, the IRT phase diagram provided by both cameras is consistent with standard calorimetric method measurements. All transitions found in the literature and detected by our DSC measurements are also depicted by the IRT method and using each camera. In a similar way as in the PA + SA system, additional transitions are detected using the IRT method but are either not corroborated by DSC analyses or are not found consistently enough to certify the occurrence of the transition. Those transitions are not included in the quantitative assessment and will be the object of further analyses.

The accuracy and reliability of the horizontal transitions and the liquidus line detection are, respectively, evaluated in Tables 5 and 6.

The average temperature deviation for the horizontal transitions detection between DSC measurements and the results provided by the FLIR photon detector using the IRT method

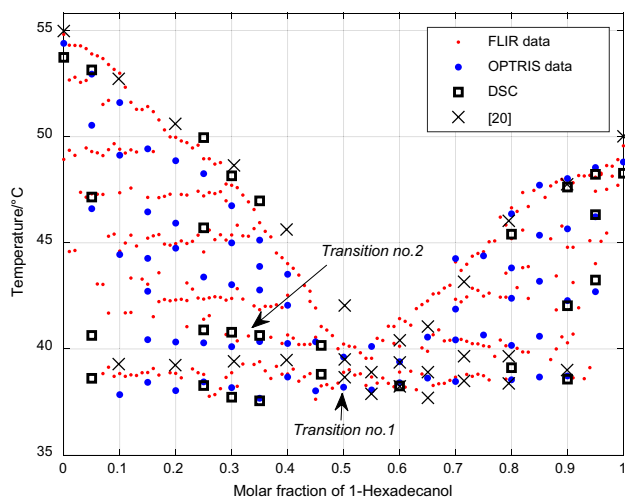


Fig. 3 Phase diagram of the HD+MA binary systems plotted using the IRT method and standard calorimetry methods

Table 5 Comparison of the horizontal transitions detection between the IRT method and DSC measurements for the HD+MA binary system

Transition no.	1	2
$\bar{T}_{\text{DSC}}/^{\circ}\text{C}$	38.37	40.743
$\sigma_{\text{DSC}}/^{\circ}\text{C}$	0.528	0.127
n	8	4
$\bar{T}_{\text{OPTRIS}}/^{\circ}\text{C}$	38.31	40.297
$\sigma_{\text{OPTRIS}}/^{\circ}\text{C}$	0.329	0.11
n	15	6
$\bar{T}_{\text{FLIR}}/^{\circ}\text{C}$	38.665	40.666
$\sigma_{\text{FLIR}}/^{\circ}\text{C}$	0.35	0.481
n	62	14

With \bar{T} the average transition temperature, σ the standard deviation and n the number of samples for which the transition is detected

is evaluated at $0.19\text{ }^{\circ}\text{C}$. The value of this deviation with the OPTRIS device reaches $0.25\text{ }^{\circ}\text{C}$. The accuracy provided by both imaging devices for this system is particularly close to DSC measurements. As for the reliability of this detection, the measured standard deviations are within range of what DSC can provide.

As for the depiction of the liquidus line provided by the IRT method, the low-cost microbolometer provides this time a slightly better approximation with an overall average temperature difference of $0.85\text{ }^{\circ}\text{C}$ against $1.03\text{ }^{\circ}\text{C}$ for the FLIR camera. Both are nonetheless relatively good estimations considering the acceptable standard deviation and the fact that the comparison is limited to the samples studied with DSC. Indeed, the FLIR data including 101 compositions can be accurate overall while allowing deviations locally. In fact, if we observe Fig. 3, we notice that the $37\text{--}42\text{ }^{\circ}\text{C}$ temperature range is an area dense in transitions for the 60% HD + 40% MA sample. DSC results found in [20] corroborate our observations using the IRT method, but our DSC analysis fails to make the distinction between the supposed

Table 6 Comparison of the liquidus line detection between the IRT method and DSC measurements for the HD+MA binary system

Comparison	DSC/OPTRIS	DSC/FLIR	OPTRIS/FLIR
$\overline{\Delta T}/^{\circ}\text{C}$	0.849	1.034	0.823
$\sigma_{\overline{\Delta T}}/^{\circ}\text{C}$	0.603	0.801	0.609
$\Delta T_{\text{max}}/^{\circ}\text{C}$	1.85	3.17	2.03
$\Delta T_{\text{min}}/^{\circ}\text{C}$	0.17	0.14	0.06
n	11	11	21

With $\overline{\Delta T}$ the average liquidus temperature difference between methods, $\sigma_{\overline{\Delta T}}$ the standard deviation, ΔT_{max} and ΔT_{min} , respectively, the maximum and minimum liquidus temperature deviation between methods and n the number of samples for which data are available with both methods

successive transitions. Moreover, the interpretation of DSC curves for systems presenting fatty acids and for narrow temperature ranges has been reported to be rather difficult [21]. The phase diagrams of fatty acids mixtures have actually been reevaluated at several occasions such as between [22, 23] where the liquidus temperature at the 50% MA + 50% SA composition is lowered by about 2.5 °C. Consequently, locally measuring high maximum temperature deviation in comparison with the rest of the phase diagram is not surprising and should not be a concern as long as the average temperature deviation and the standard deviation remain at acceptable levels. It also suggests that those higher deviations recorded between DSC and IRT may not be caused by the IRT method, especially given the low and consistent deviation present between results obtained with both cameras.

1-Hexadecanol + 1-octadecanol

The phase diagram obtained applying the IRT method using both cameras is plotted in Fig. 4 where it is compared to the phase diagram and transitions detected with DSC measurements as well as in the literature [24]. The purity of both pure compounds in literature and in this work is comparable.

The phase diagram obtained applying the IRT method for the HD + OD binary system matches the results found in the literature and the ones obtained using DSC measurements. We once again notice that additional transitions are detected with the infrared cameras that need confirmation

by confrontation to other standard methods (such as X-ray diffraction).

The accuracy and reliability of the horizontal transitions and the liquidus line detection are, respectively, evaluated in Tables 7 and 8.

The lowest transition in Fig. 4 (i.e., Transition 1) has been detected on a very consistent basis both using the IRT method and with DSC measurements. However, it is difficult to say whether it consists in a single transition or a combination of multiple ones without further analysis. Therefore, it has been preferred not to consider this transition.

Table 7 Comparison of the horizontal transition detection between the IRT method and DSC measurements for the HD + OD binary system

Transition no.	2
$\bar{T}_{DSC}/^{\circ}C$	34.875
$\sigma_{DSC}/^{\circ}C$	0.326
n	4
$\bar{T}_{OPTRIS}/^{\circ}C$	33.107
$\sigma_{OPTRIS}/^{\circ}C$	0.985
n	59
$\bar{T}_{FLIR}/^{\circ}C$	34.151
$\sigma_{FLIR}/^{\circ}C$	0.725
n	59

With \bar{T} the average transition temperature, σ the standard deviation and n the number of samples for which the transition is detected.

Fig. 4 Phase diagram of the HD + OD binary systems plotted using the IRT method and standard calorimetry methods

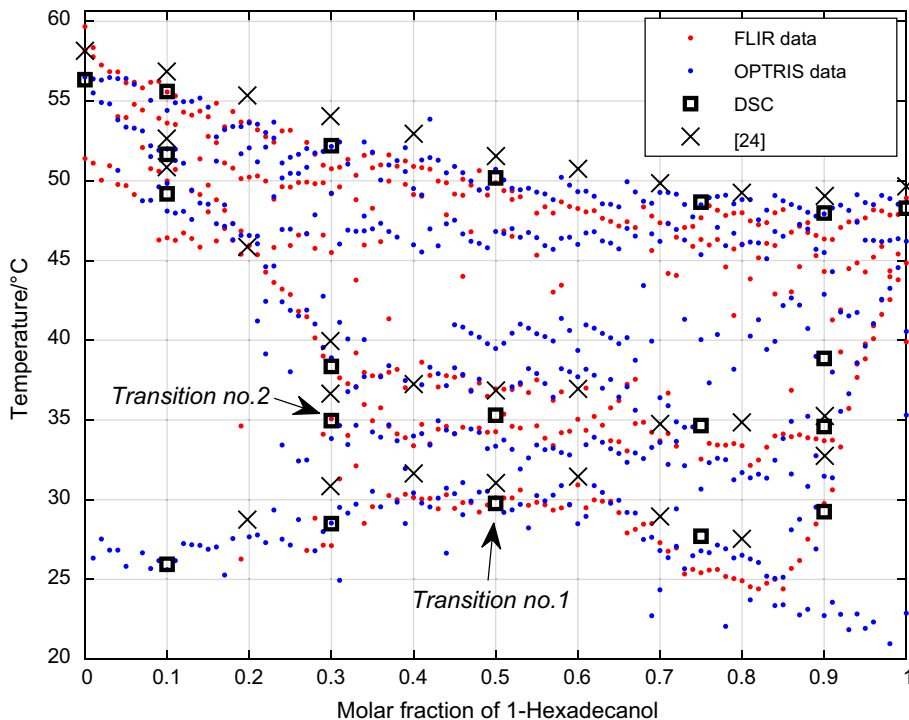


Table 8 Comparison of the liquidus line detection between the IRT method and DSC measurements for the HD + OD binary system

Comparison	DSC/OPTRIS	DSC/FLIR	OPTRIS/FLIR
$\overline{\Delta T}/^{\circ}\text{C}$	0.364	1.197	0.975
$\sigma_{\overline{\Delta T}}/^{\circ}\text{C}$	0.404	1.102	0.611
$\Delta T_{\text{max}}/^{\circ}\text{C}$	1.187	3.329	2.702
$\Delta T_{\text{min}}/^{\circ}\text{C}$	0.049	0.036	0.051
n	7	7	96

With $\overline{\Delta T}$ the average liquidus temperature difference between methods, $\sigma_{\overline{\Delta T}}$ the standard deviation, ΔT_{max} and ΔT_{min} , respectively, the maximum and minimum liquidus temperature deviation between methods and n the number of samples for which data is available with both methods

Consequently, only one horizontal transition is considered for this system. It should be mentioned that this transition is located in an area dense in transitions. The IRT data suggest that two transitions occur successively with a narrow temperature interval and that our DSC measurements support the presence of the lower one while the literature favors the upper one. The comparison is therefore only made for the transition supported by our DSC measurements. The temperature deviation between the IRT method using the OPTRIS camera and DSC measurements is 1.77 °C, while the FLIR provides a 0.72 °C deviation. The high-end photon detector hence provides a better accuracy than the low-cost microbolometer in this particular case. However, the comparison is made between standard method measurements based on 4 points whereas both cameras provided a transition made of 59 points. It suggests that the transition detected using the IRT method is more likely to depict a correct transition shape and that the reliability of the reading is potentially erroneous given the dense transition area. The higher standard deviations computed for the detection of this transition using the IRT method support this assessment.

On the contrary to the horizontal transition detection, the OPTRIS microbolometer shows significantly better liquidus line detection accuracy with a temperature deviation of only 0.36 °C against 1.2 °C for the FLIR camera. Although 1.2 °C deviation is not bad for a first estimation, it should be mentioned that once again the comparison is made based on the 7 samples that were studied using the DSC. Considering the low number of comparative points, it is likely to have local deviations significantly alter the end result. In fact, if we observe the measured maximum temperature deviation, we see that a maximum deviation of 3.33 °C was measured for the DSC/FLIR comparison whereas this deviation only reaches 1.19 °C for the DSC/OPTRIS comparison. This assessment combined with the higher standard deviation obtained for the DSC/FLIR comparison suggests that the value obtained with the FLIR camera could have been significantly different if slightly different compositions

were considered. This assessment is confirmed if we look at the comparison of the results obtained between the two cameras. Although the overall temperature deviation is estimated at 0.98 °C, the standard deviation is relatively low, suggesting that a simple offset exists between both depicted liquidus lines. A closer look at the maximum deviation of the recorded temperature shows, upon comparison of 96 samples, that the maximum deviation is estimated at 2.7 °C which is lower than the deviation measured between the DSC and only based on 7 samples.

Myristic acid + stearic acid

The phase diagram obtained applying the IRT method using both cameras is plotted in Fig. 5 where it is compared to the phase diagram and transitions detected with DSC measurements as well as in the literature [22]. The purity of the pure myristic acid in the literature and in this work is comparable, but the stearic acid one is slightly better in the present study. As a result, DSC measurements and literature data may not fully coincide.

Once again, using the IRT method and for both infrared cameras, the obtained phase diagram is consistent with the results from literature and DSC measurements. In the 52–60 °C temperature range, several transitions seem to successively take place. In that range, the literature and our DSC measurements report a transition whose occurrence either is not detected consistently using the infrared cameras or could be mistaken for another transition detected using the IRT method only. It was chosen not to consider this transition (i.e., transition 3) in order to avoid erroneous conclusions. Although the transitions detected with the IRT method between 55 and 60 °C could not be confirmed

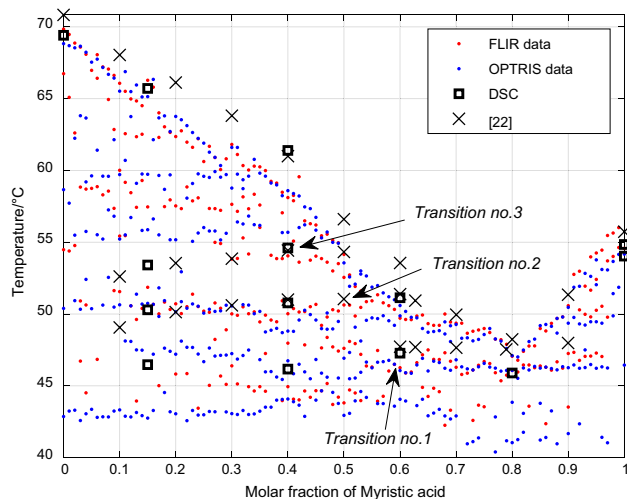


Fig. 5 Phase diagram of the MA + SA binary systems plotted using the IRT method and standard calorimetry methods

with the DSC, the detection appears relatively consistent and hints toward the occurrence of possible transitions. This phenomenon, particularly noticeable for this system, actually appears locally in the previous presented systems. This aspect will be discussed later on as it may bring valuable information.

The accuracy and reliability of the horizontal transitions and the liquidus line detection are, respectively, evaluated in Tables 9 and 10.

The average temperature deviation for the detection of the horizontal transitions using the FLIR photon detector is 0.18 °C in comparison with DSC measurements. The obtained value of this deviation with the OPTRIS microbolometer is 0.35 °C. Here again, both show incredible accuracies even though the high-end camera is slightly more precise. As for the detection accuracy, the IRT method for both cameras provides standard deviation in the range of the DSC one and for a significantly greater amount of samples.

Regarding the accuracy and reliability of the liquidus line detection using the IRT method with both cameras, we can

Table 9 Comparison of the horizontal transitions detection between the IRT method and DSC measurements for the MA + SA binary system

Transition no.	1	2
$\bar{T}_{DSC}/^{\circ}C$	46.448	50.53
$\sigma_{DSC}/^{\circ}C$	0.597	0.339
n	4	2
$\bar{T}_{OPTRIS}/^{\circ}C$	46.381	49.893
$\sigma_{OPTRIS}/^{\circ}C$	0.508	0.663
n	76	57
$\bar{T}_{FLIR}/^{\circ}C$	46.387	50.229
$\sigma_{FLIR}/^{\circ}C$	0.665	0.407
n	56	47

With \bar{T} the average transition temperature, σ the standard deviation and n the number of samples for which the transition is detected

Table 10 Comparison of the liquidus line detection between the IRT method and DSC measurements for the MA + SA binary system

Comparison	DSC/OPTRIS	DSC/FLIR	OPTRIS/FLIR
$\overline{\Delta T}/^{\circ}C$	1.062	1.19	0.578
$\sigma_{\overline{\Delta T}}/^{\circ}C$	0.888	1.116	0.489
$\Delta T_{max}/^{\circ}C$	2.8	3.28	2.4
$\Delta T_{min}/^{\circ}C$	0.54	0.27	0
n	6	6	101

With $\overline{\Delta T}$ the average liquidus temperature difference between methods, $\sigma_{\overline{\Delta T}}$ the standard deviation, ΔT_{max} and ΔT_{min} , respectively, the maximum and minimum liquidus temperature deviation between methods and n the number of samples for which data is available with both methods

see that the obtained results are highly comparable. Both the overall temperature deviation and the standard deviation are around 1 °C with a maximum temperature deviation of approximately 3 °C for a comparison based on 6 samples only. It should also be mentioned that this system is the one from [22], previously mentioned, reevaluated in [23] because of its complexity [21–23]. These maximum temperature deviations should consequently not to be of too much concern given the relatively good overall accuracy and low amount of tested samples. This leads toward the same conclusions than for the previous system that although the accuracy is satisfactory, more reliable results could have been obtained for different samples or with significantly more tested samples. The comparison of the results obtained using both cameras also suggests this assessment. Indeed, we see that both the overall temperature deviation and the standard deviation are relatively low and that a maximum temperature deviation of 2.4 °C is measured over 101 tested compositions.

Discussion

The previous results show that the low-cost OPTRIS microbolometer allows providing results in the range, if not better, of the high-end cooled FLIR photon detector when used for phase diagram estimation of binary systems of fatty acids and fatty alcohols using the IRT method. It has been shown that, with transition detection accuracy around or below 1 °C and standard deviations in the range of our DSC measurements, both cameras are able to render a consistent phase diagram. However, it has been reported for all systems that small and consistent deviations exist between the results obtained using both cameras, suggesting that the IRT method depicts the same phase diagram with both cameras. We also see that although the temperature deviation between the IRT method and DSC measurements is rather low, it is inconsistent with the comparison made between cameras. Given the larger standard deviations obtained, it is more likely that the error induced is local and dependent on the sample studied. In fact, it was shown that the maximum temperature deviation is often found for compositions presenting several successive and close transitions. In that context, it is not surprising to find irregularities between results given by different methods especially if they are based on significantly different principles. This aspect can be illustrated by Fig. 6 where a comparison is made between signals obtained using the IRT method and a DSC curve for a sample of pure SA. The interpretation of the DSC curve is made using rigorous guidelines [18] stipulating when to consider onset or peak temperature as transition temperature. For this given example, the onset temperature would be considered and

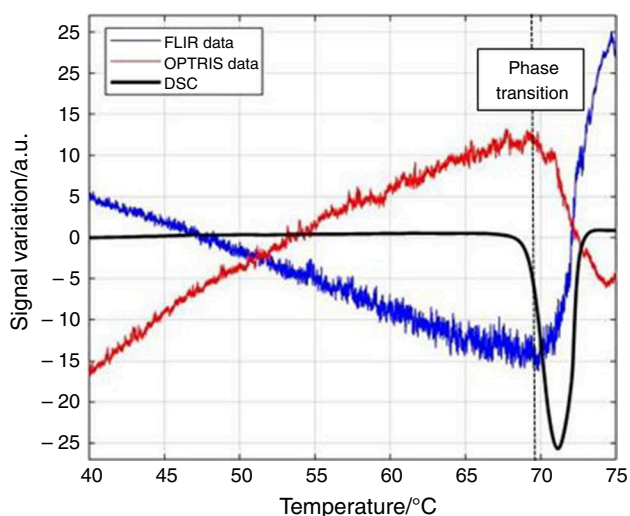


Fig. 6 Comparison between the IRT data and a DSC curve for a pure sample of SA

as can be noticed, the abrupt variation in the infrared signals coincides with the onset temperature of the DSC curve. However, if several transitions were to occur, a clear reading of the onset temperature cannot always be made and in that case, the peak temperature is considered. This matter is illustrated via a DSC curve available in the Supplementary material. As the IRT method relies on visual observation, it can detect not only heat exchanges but also morphological or structural changes in a sample. It may allow the reading of onset temperatures even in the case of successive transitions. Although further analyses with other standard methods are needed to confirm this assumption, it may be a real asset for the IRT method as onset temperature are usually more representative of the beginning of a phase change process. If confirmed, it may explain the significant recorded local deviations. In addition, it should be noted that the studied systems were purposefully selected because of their complex nature in order to test the limits of the IRT method. In fact, the phase diagrams of fatty acids are particularly complex and were reevaluated at several occasions [19, 21–23, 25]. Given those difficulties, the IRT method may have brought insightful information regarding the phase diagrams of fatty acids with several undocumented transitions that should as well be investigated further. In fact, a closer look at Figs. 2–5 shows multiple transitions that could be related to polymorphic transitions as presented in [26, 27] and solid solubility domains as presented in [19, 20, 22, 24]. Those transitions are usually very challenging to identify and require the use of various expensive and time-consuming methods (i.e., X-ray powder diffraction, scanning electron microscopy,

Fourier transform infrared spectroscopy, etc.) to confirm their occurrence. In that frame, the IRT method could represent a real asset and a promising complement to standard calorimetric methods.

Besides, when predicting the impact of the camera specifications on the results provided by the IRT method, it was suggested that of all the characteristics listed in Table 2, the OPTRIS microbolometer has the advantage of having a high spectral range (7.5–13 μm) particularly adapted for applications under 150 $^{\circ}\text{C}$ because of the higher spectral radiance [15, 17]. On the other hand, the cooled InSb FLIR photon detector is characterized by a higher detectivity [15]. Regarding the higher detectivity of the FLIR camera, it may explain the better performances for the detection of horizontal transitions. Given that the latter often have lower energies than liquidus transitions, it might have been advantageous. However, the performances of the microbolometer are not far behind, even better in some instances as for the liquidus line detection. In that situation, we may consider that it is more suitable to have a fitting spectral range than a high detectivity. Additionally, if one were to consider the use of a photon detector with a higher spectral range, it should be noted that the difference in detectivities between bolometers and photon detector becomes less noticeable for higher spectral ranges [15] and that the gain in performance may not justify the significant price difference especially considering the highly satisfying performances of the low-cost microbolometer.

Conclusions

The study of the influence of the infrared camera choice on the results obtained using the IRT method was performed. Two infrared cameras with significantly different properties at drastically different prices were used for the phase diagram estimation of four binary systems of fatty acids and fatty alcohols: (1) the FLIR X6580 SC, a cooled photon detector and (2) the OPTRIS PI 450, an uncooled low-cost microbolometer. The phase diagrams provided by the IRT method for both cameras presented slight to no differences and the accuracy and reliability of the transition detection were correct in both cases. Given the significant difference in the economic impact in the use of the IRT method for phase diagram estimation, it makes no doubt that a low-cost microbolometer is a suitable option for the aimed application. The IRT method shows to be a fast and reliable phase diagram estimation method, allowing the simultaneous testing of 101 compositions in a single experiment while providing a considerably cheaper alternative to the existing

standard methods. On top of that it has proven to be able to provide accurate transitions depiction with a low-cost experimental setup. Although satisfactory results were provided, several improvement points are to be discussed. The infrared data interpretation has to be compared to other methods so that the obtained phase diagrams are built on rigorous and consistent guidelines. The assessment of the influence of operating conditions must be continued to ensure low time consumption, satisfactory performances and the lowest cost. Additionally, the assessment was performed for phase diagrams estimations for low temperature applications. A similar assessment may be required if applications at higher temperatures are required. Finally, it has been identified that further analyses using other standard methods were needed to assess the accuracy of the IRT method when large local deviations were measured and to confirm the occurrence and nature of additional detected transitions.

Acknowledgements This work is carried out in the frame of SUDOKET project and is co-funded by the Interreg Sudoe Programme through the European Regional Development Fund (ERDF). The authors acknowledge them as well as the financial support of Region Nouvelle Aquitaine for subsidizing BioMCP project (Project-2017-1R10209-13023). We also would like to thank CNRS for promoting the I2M Bordeaux—CICe exchanges in the framework of the PICS PHASE-IR project.

References

- Campbell FC. Phase diagrams: understanding the basics. Cleveland: ASM International; 2012.
- Institute for Materials Research (U.S.), National Measurement Laboratory (U.S.). Office of Standard Reference Data, National Science Foundation (U.S.). Applications of phase diagrams in metallurgy and ceramics: proceedings of a Workshop Held at the National Bureau of Standards, Gaithersburg, Maryland, January 10–12, 1977.
- Dubost B. Industrial applications and determination of equilibrium phase diagrams for light alloys. Progress and prospects. *Rev Met Paris*. 1993;90(2):195–21010.
- Yang Y, Bewlay BP, Chen S, Chang YA. Application of phase diagram calculations to development of new ultra-high temperature structural materials. *Trans Nonferrous Met Soc China*. 2007;17(6):1396–404.
- Palomo Del Barrio E, Cadoret R, Daranlot J, Achchaq F. Infrared thermography method for fast estimation of phase diagrams. *Thermochim Acta*. 2016;625:9–19.
- Mailhé C, Duquesne M, Palomo del Barrio E, Azaiez M, Achchaq F. Phase diagrams of fatty acids as biosourced phase change materials for thermal energy storage. *Appl Sci*. 2019;9(6):1067.
- Mailhé C, Duquesne M, Mahroug I, Palomo Del Barrio E. Improved infrared thermography method for fast estimation of complex phase diagrams. *Thermochim Acta*. 2019;675:84–91.
- Midgley C, LMC International. The market outlook for fatty acids. ICIS Pan American Oleochemical Conference, October 2018.
- OCDE, FAO. OECD-FAO Agricultural Outlook 2019–2028. Paris: OCDE Editions; 2019.
- Maximo GJ, Costa MC, Coutinho JAP, Meirelles AJA. Trends and demands in the solid–liquid equilibrium of lipidic mixtures. *RSC Adv*. 2014;4(60):31840–50.
- Liu P, Gu X, Bian L, Peng L, He H. Capric acid/intercalated diatomite as form-stable composite phase change material for thermal energy storage. *J Therm Anal Calorim*. 2019;138(1):359–368–368. <https://doi.org/10.1139/f00-225>.
- Hussain SI, Kalaiselvam S. Nanoencapsulation of oleic acid phase change material with Ag₂O nanoparticles-based urea formaldehyde shell for building thermal energy storage. *J Therm Anal Calorim*. 2019. <https://doi.org/10.1007/s10973-019-08732-5>.
- Liu Z, Jiang L, Fu X, Zhang J, Lei J. Preparation and characterization of n-octadecane-based reversible gel as form-stable phase change materials for thermal energy storage. *J Therm Anal Calorim*. 2019. <https://doi.org/10.1007/s10973-019-08975-2>.
- Gao L, Sun X, Sun B, Che D, Li S, Liu Z. Preparation and thermal properties of palmitic acid/expanded graphite/carbon fiber composite phase change materials for thermal energy storage. *J Therm Anal Calorim*. 2019. <https://doi.org/10.1007/s10973-019-08755-y>.
- Vollmer M, Möllmann K-P. Infrared thermal imaging: fundamentals, research and applications. New York: Wiley; 2011. p. 2847–59–2859. <https://doi.org/10.1890/04-1455>.
- Syllaios A.J, Ha M, McCardel W, Schimert T. Measurement of thermal time constant of microbolometer arrays. In: Proceedings of the SPIE 5783, infrared technology and applications XXXI (31 May 2005)
- Hobday AJ, Smith ADM, Stobutzki IC, Bulman C, Daley R, Dambacher JM, Deng RA, Dowdney J, Fuller M, Furlani D, Griffiths SP, Johnson D, Kenyon R, Knuckey IA, Ling SD, Pitcher R, Sainsbury KJ, Sporcic M, Smith T, Turnbull C, Walker TI, Wayte SE, Webb H, Williams A, Wise BS, Zhou S. Infrared thermography for temperature measurement and non-destructive testing. *Sensors*. 2014;14:12305–48–12348. <https://doi.org/10.1016/j.fishres.2011.01.013>.
- Boettinger WJ, Kattner UR, Moon K-W, Perepezko JH. Chapter V—DTA and heat-flux DSC measurements of alloy melting and freezing. In: Zhao JC, editor. Methods for phase diagram determination. Oxford: Elsevier Science Ltd; 2007. pp. 151–221.
- Costa MC, Sardo M, Rolemberg MP, Coutinho JAP, Meirelles AJA, Ribeiro-Claro P, et al. The solid–liquid phase diagrams of binary mixtures of consecutive, even saturated fatty acids. *Chem Phys Lipid*. 2007;160(2):85–97.
- Maximo GJ, Carareto NDD, Costa MC, dos Santos AO, Cardoso LP, Krähenbühl MA, et al. On the solid–liquid equilibrium of binary mixtures of fatty alcohols and fatty acids. *Fluid Phase Equilib*. 2014;366:88–98.
- Rolemberg MP. Equilíbrio sólido–líquido de ácidos graxos e triglicerídeos: determinação experimental e modelagem. 2002.
- Costa MC, Sardo M, Rolemberg MP, Ribeiro-Claro P, Meirelles AJA, Coutinho JAP, et al. The solid–liquid phase diagrams of binary mixtures of consecutive, even saturated fatty acids: differing by four carbon atoms. *Chem Phys Lipid*. 2009;157(1):40–50.
- Maximo GJ, Aquino RT, Meirelles AJA, Krähenbühl MA, Costa MC. Enhancing the description of SSLE data for binary and ternary fatty mixtures. *Fluid Phase Equilib*. 2016;426:119–30. <https://doi.org/10.1093/conphys/cov059>.
- Carareto NDD, Costa MC, Meirelles AJA, Pauly J. High pressure solid-liquid equilibrium of fatty alcohols binary systems from 1-dodecanol, 1-tetradecanol, 1-hexadecanol, and 1-octadecanol. *J Chem Eng Data*. 2015;60(10):2966–73.

25. Costa MC, Rolemberg MP, Boros LAD, Krähenbühl MA, de Oliveira MG, Meirelles AJA. Solid–liquid equilibrium of binary fatty acid mixtures. *J Chem Eng Data*. 2007;52(1):30–6.
26. Gbabode G, Negrier P, Mondieig D, Moreno E, Calvet T, Cuevas-Diarte MA. Fatty acids polymorphism and solid-state miscibility: pentadecanoic acid–hexadecanoic acid binary system. *J Alloys Compd*. 2009;469(1):539–51.
27. Moreno E, Cordobilla R, Calvet T, Cuevas-Diarte MA, Gbabode G, Negrier P, et al. Polymorphism of even saturated carboxylic acids from n-decanoic to n-eicosanoic acid. *New J Chem*. 2007;31:947–57.

Publisher's Note Springer Nature remains neutral with regard to jurisdictional claims in published maps and institutional affiliations.